ATLAS NOTE

XXX-2015-XXX

2nd April 2015

Draft version 1.0

Dark matter models coupled to the top quark and discovery potential at LHC

Barbara Alvarez Gonzalez[a], Romain Madar[b], Théo Megy[b]

[a] *CERN (Geneva, SWITZERLAND)*
[b] *Laboratoire de Physique Corpusculaire (Clermont-Ferrand, FRANCE)*

Abstract

This document presents different dark matter models that couple to the top quark, leading to monotop and same sign top pair production. The main ingredients of each models will be described, as well as the different assumptions and simplifications needed to derive a well defined collider phenomenology. The search strategy and the discovery potential at the LHC will be also discussed for each of these models.

Contents

1. Motivations and models description

In this note, we describe the phenomenology of dark matter models involving a strong coupling to the top quark. These models can be classified according to their experimental signatures. Assuming the Standard Model (SM) flavour scheme, the models essentially lead to $t\bar{t} + E_{\mathrm{T}}^{\mathrm{miss}}$ final state and are described in a separated document. Since we do not know the flavour structure of the dark sector, it is also interesting to relax this constraint and consider a different experimental signatures: monotop final state ($t + E_{\mathrm{T}}^{\mathrm{miss}}$) and a prompt production of two top quarks having the same electric charge (tt)[1]. These two final states are forbidden at the leading order in the SM and become thus a good area to search for any new physics, and in particular dark matter.

1.1. Model structure

As usual, a dark matter candidate χ and a mediator M (vectorial or scalar) need to be added to the SM to describe the dark sector and its interaction with the SM particles. The full details of the various models are described in [1, 2], the basic ingredients are the following:

1. the theory is effective and respects the $\mathrm{SU}(2)_L \times \mathrm{U}(1)_Y$ symmetry,
2. the mediator strongly couples to the top quark,
3. the top quark is *singly* produced in association with a new particle X_{new} (dark matter or mediator).

There are two classes of models based on the monotop production mode: resonant and non-resonant production, as shown in Fig. 1. The sections 1.1.1 and 1.1.2 describe the phenomenology leading to such production mechanisms. Depending on the nature of X_{new}, two main final states might be relevant: monotop production or same-sign top quark pair production. Section 2 discusses how the interplay of these two signatures can largely probe this class of dark matter model.

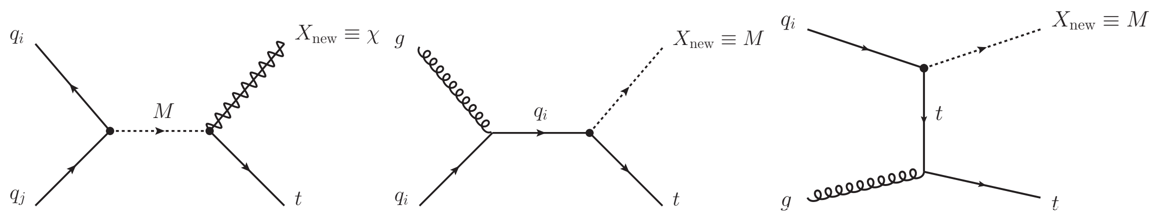

Figure 1: Feynman diagram of leading order processes leading to monotop events: resonant production of t via resonant mediator M decaying into a top quark and X_{new}, which is the dark matter fermion χ (left), and s and t channel non-resonant production of a top quark in association with X_{new}, which is the mediator M (middle and right).

1.1.1. Resonant production

In this case, the mediator M is a couloured 2/3-charged scalar $\phi^{\pm}$ decaying into a top quark and a spin-1/2 invisible particle, χ (X_{new} is then the dark matter candidate χ). The dynamics of the new sector is then

[1] For simplicity, the notation tt is used to describe both tt and $\bar{t}\bar{t}$

described by the following lagrangian:

$$\mathcal{L}_{\rm int} \;=\; d_i^C \;\left[\left(g^v_{\phi d}\right)^{ij} + \left(g^a_{\phi d}\right)^{ij}\gamma^5\right] \; d_j\;\phi^\pm \;+\; u_k^C\left[\left(g^v_{u\chi}\right)^{k} + \left(g^a_{u\chi}\right)^{k}\gamma^5\right]\;\chi\;\phi^\pm \tag{1}$$

where u (d) stands for any *up*-quark (*down*-quark), the index v (a) stands for vectorial (axial), C means charge conjugate and i, j, k run over the generations (color indices involved in the $\phi^\pm$−quarks interaction are not explicitly written). The first term leads to the production of the mediator and the last term allows its decay into a *up*-quark and a non interacting fermion (in particular to the top quark when $\left(g^{v/a}_{u\chi}\right)^k$ is sizable mainly for $k = 3$). This model is then described by the masses of the mediator m_ϕ and the invisible fermion m_χ, and the coupling $\left(g^{v/a}_{\phi d}\right)^{ij}$ and $\left(g^{v/a}_{u\chi}\right)^k$.

Question/comment: in this resonant model, this is not so obvious to interpret $\phi_\pm$ as the mediator since there is a vertex $\phi - u - \chi$. It is somehow breaking the concept of having a dark sector weakly coupled to ordinary matter via a mediator.

1.1.2. Non-resonant production

For the non-resonant production, the top quark is produced in association with the mediator ($X_{\rm new}$ is then the mediator and not the dark matter candidate). They are two possibilities depending on the nature of the mediator.

First, the mediator can be a scalar field interacting with the SM field and the dark matter candidate as described in this lagrangian:

$$\mathcal{L}_{\rm int} \;=\; u_i^C \;\left[\left(g^v_{\phi u}\right)^{ij} + \left(g^a_{\phi u}\right)^{ij}\gamma^5\right] \; u_j\;\phi \;+\; \chi^C\left[g^v_{\phi\chi} + g^a_{\phi\chi}\gamma^5\right]\chi\;\phi \tag{2}$$

where u stands for any *up*-quark, the index v (a) stands for vectorial (axial), C means charge conjugate and i, j, k run over the generations. The first term describes the interaction between the mediator and the *up*-quarks while the second term leads to the decay the mediator into invisible fermions. In this model, there is necessarily a mixing between ϕ and the Higgs boson field. Additional parameters are then required to describe this new sector. Indeed, on top of the mediator mass and couplings, the mixing matrix of the two scalar fields is needed in order to make predictions. For the sake of simplicity, we do not consider this case were the parameters space would be too large.

Another possibility is to consider a vectorial field as mediator with the following dynamics:

$$\mathcal{L}_{\rm int} \;=\; \bar{u}_i\left[\left(g^v_{Vu}\right)^{ij}\gamma^\mu + \left(g^a_{Vu}\right)^{ij}\gamma^5\right]u_j\;V_\mu \;+\; \bar{\chi}\left[g^v_{Vu}\gamma^\mu + g^a_{V\chi}\gamma^5\right]\chi\;V_\mu \tag{3}$$

where u stands for any *up*-quark, the index v (a) stands for vectorial (axial) and i, j, k run over the generations. The first term describes the interaction between the mediator and the *up*-quarks while the second term leads to the decay the mediator into invisible fermions. The new sector can be defined with the couplings $\left(g^{v/a}_{Vu}\right)^{ij}$, $g^{a/v}_{V\chi}$ and the masses m_V and m_χ. This model can be probed by two experimental signatures depending on the exact scenario: monotop and same-sign top quark production.

Question for theorists: why it cannot mix with Z in case of vectorial mediator ?

1.2. Simplifications

The lagrangians from equations (1) and (3) contains too many degrees of freedom, which makes the LHC phenomenology difficult to predict. In addition, only a certain region of the parameter space can actually be probed with a monotop final state. For these reasons, further simplifications are performed in particular in term of flavour and chiral structure of the model. These simplifications leads to some limitations in the way ATLAS and CMS can constrain the model parameter space and these limitations are also qualitatively discussed below.

1.2.1. Flavour structure

The flavour structure is simplified in order to have a reasonable signal production rate in proton-proton collisions. In case of a scalar mediator, it has to be sufficiently produced so it has to couple with proton content, namely lightest quark which are allowed in equation (1). The monotop final state is sensitive to the scenario where ϕ strongly couples to $t\chi$. Correct and/or complete with the monotop paper. In term of parameter space, it means that the monotop final state is not sensitive to some parameters like coupling between the mediator and heavy quarks or the scenario in which BR$(\phi \to t\chi) \ll 100\%$. For the latest, there is a way to recover the sensitivity looking at $u_i d_j \to \phi \to u_i d_j$. Since ϕ must be produced, it has to coupled to quarks and must decay in the same final state. Experimentally, this would correspond to a di-jet resonance search.

The same kind of simplification is performed for the non-resonant production. The equation (3) is simplified in the parameter space where a monotop final state can be sufficiently produced to be detected at the LHC. The mediator V must be produced from light quark initial state, in association with a top quark: this signature can mainly probe a high coupling $\left(g^{v/a}_{Vu}\right)^{13}_{Vu} \equiv g^{v/a}_{Vtu}$. Therefore, the sensitivity to other flavour couplings is significantly lower since V is less importantly produced. In addition, the mediator must decay into invisible particles to lead to the searched monotop final state. As a consequence, the sensitivity for scenario where BR$(V \to \chi\chi) \ll 100\%$ can be quite low. To cope with this second limitation, a same-sign top quark final state $gu \to tV(\to t\bar{u})$ is proposed to cover the cases where V would decay into visible particles. This case is more likely as the tV production rate increases, and becomes then a key point to constraint this model in a consistent way.

Questions for theorists:

- How well these flavour assumptions are allowed by the other HEP data (proton decay life time, flavour physics, etc ...) ?
- MFV criteria ?

1.2.2. Chiral structure

The main point here is to consider only right handed quark components in order to not simplify the phenomenology. In fact, the representation of the left-handed components under the SU$(2)_L$ symmetry imposes a coupling to *down*-type quarks, since the effective theory is invariant under SU$(2)_L \times$ U$(1)_Y$ gauge symmetry. Having a coupling between the mediator and *down*-type quarks fairly complicates the collider phenomenology in term of decay mode. Typically, including the left-handed components of quarks in the lagrangian (3) describing the Vtu vertex would lead to

$$\mathcal{L}_{Vtu} = g^R_{Vtu}\, \bar{t}_R \gamma^\mu u_R\, V_\mu + g^L_{Vtu} \left(\bar{t}_L \gamma^\mu u_L + \bar{b}_L \gamma^\mu d_L \right) V_\mu \tag{4}$$

where $g^{R/L} \equiv 1/2\,(g^v \pm g^a)$ couples only to right-handed/left-handed components. The second term ensure the invariance under $SU(2)_L$ rotations, and lead to an additional decay mode $V \to b\bar{d} + \bar{b}d$ (on top of $V \to t\bar{u} + \bar{t}u$ and $V \to \chi\chi$).

1.3. Notations

In section 2, the collider phenomenology and benchmark definition is discussed with notations which are a bit different[2] from section 1. This section describes the notations used in section 2 as well as the MadGraph model [3] convention, in term of the ones introduced in section 1.

The Madgraph model corresponds to the Lagrangian from [1]. Each coupling constant of this dynamics can be set via the paramater card and the blocks which are relevant for the two models used in section 2 are described below.

1. Resonant scalar model described by the Lagrangian (1)
   - `AQS` and `BQS`: 3×3 matrices (flavour space) fixing the coupling of the scalar $\phi^\pm$ (S stands for scalar) and *down*-type quarks (Q stands for quarks), written in this note $g_{\phi u}$ or a^q_{res}.
   - `A12S` and `B12S`: 3×1 matrices (flavour space) fixing the coupling of the fermion χ (12 stands for spin-1/2 fermion) and *up*-type quarks, written in this note $g_{u\chi}$ or $a^{1/2}_{\text{res}}$.
   - particle name: the scalar $\phi^\pm$ is labelled S and the fermion χ is f_{met}
2. Non-resonant vectorial model described by the Lagrangian (3)
   - `A1FC` and `B1FC`: 3×3 matrices (flavour space) fixing the coupling of the vector V (1 stands for vector) and *up*-type quarks, written in this note g_{Vu} or $a_{\text{non-res}}$.
   - particle name: the vector V is labelled v_{met} and the fermion χ doesn't exist
   - the dark matter candidate χ is not implemented (this model assumes $\text{BR}(V \to \chi\chi) = 100\%$)

A means vectorial coupling (g^v) and B means axial coupling (g^a) and these two matrices are taken to be equal according to the chiral simplification (see section 1.2.2). The convention used in [4] and in section 2.1.1 is to define a single number a_{res} ($a_{\text{non-res}}$) for the resonant (non resonant) model, such as $(a^q_{\text{res}})_{12} = (a^q_{\text{res}})_{21} = (a^{1/2}_{\text{res}})_3 \equiv a_{\text{res}}$ (in order to have $d - s - S$ couplings, and $t - S - f_{met}$ couplings) and $(a_{\text{non-res}})_{13} = (a_{\text{non-res}})_{31} \equiv a_{\text{non-res}}$ (in order to have $v_{met} - t - u$ couplings).

[2] This difference is due to two things: the historical developpement on the monotop analysis and having a common and simple set of notations for equations (1), (2) and (3).

2. Collider signatures

As explained in Section 1, there are two types of model that can be constrained by the following signatures at the Large Hadron Collider (LHC):

1. $t + E_{\mathrm{T}}^{\mathrm{miss}}$ final state (resonant and non-resonant production)
2. $tt + X$ final state (non-resonant production)

These two productions are highly suppressed in the SM and makes these channels good candidates to search for new physics. In the current section, details about the global search strategy are given in each cases and the interplay between the two final state is described. Finally, some considerations on practical aspects are discussed, such as parameters scan or PDF and showering modeling for the signal generation.

2.1. Search strategy

2.1.1. $t + E_{\mathrm{T}}^{\mathrm{miss}}$ final state

The search performed during the LHC Run 1 with the ATLAS experiment for the production of single-top quarks in association with missing energy denoted as monotop is briefly described in this section, for more information see Ref. [4]. The search is based on the lepton+jets channel where the W boson coming from the top quark decays leptonically into an electron or a muon in association with a neutrino. The experimental signature of monotop events is given by one isolated charged lepton (electron or muon), large missing transverse energy, and one b-tagged jet as shown in Fig. 2.

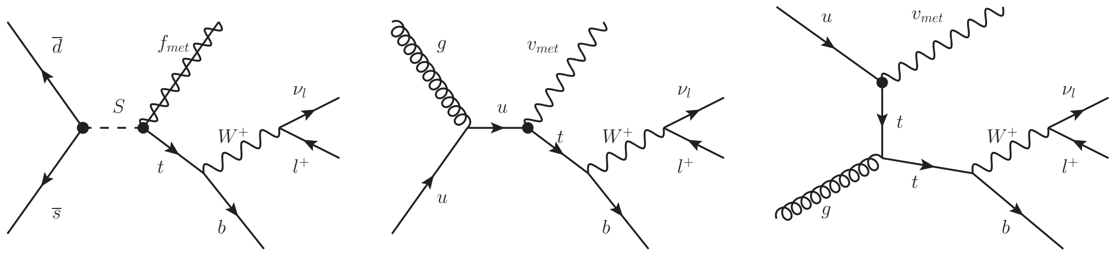

Figure 2: Feynman diagram of leading order processes leading to monotop events with a semi-leptonic topology: production of a coloured scalar resonance S decaying into a top quark and a spin-1/2 fermion f_{met} in the resonance model, and s- and t-channel non resonant production of a top quark in association with a spin-1 boson v_{met} in the non-resonance model.

The analysis strategy used in this search is based on a cut-and-count approach which is used to extract the monotop signal. The azimuthal angle difference between the charged lepton and the b-jet ($|\Delta\phi(l, b)|$) and low transverse W mass ($m_{\mathrm{T}}(W)$) are used to define the final signal regions:

- For the resonant case, the optimized signal region is $m_{\mathrm{T}}(W) > 210$ GeV and $|\Delta\phi(l, b)| < 1.2$ in addition to the signal region pre-selection
- For the non-resonant case, the optimized signal region is $m_{\mathrm{T}}(W) > 250$ GeV and $|\Delta\phi(l, b)| < 1.4$ in addition to the signal region pre-selection

The main background contributions to the signal regions is the top-antitop quark pair production ($t\bar{t}$) in particular dilepton $t\bar{t}$ events. The main systematic uncertainties are those related to the jet energy scale, the b-tagging efficiency, the effect of the choice of PDF on signal and background acceptance, the effect of the choice of Monte Carlo (MC) generator and of additional radiation on $t\bar{t}$ modelling, and the effect of the limited size of the samples.

In the absence of deviation with respect to the SM predictions, this search gives upper limits on the production cross-section at 95% confidence level (CL) for two signal models, producing right-handed top quarks together with exotic objects giving rise to missing energy. In the case of the production of a 500 GeV spin-0 resonance, the excluded effective coupling is below a_{res}= 0.15, for a mass of the invisible spin-1/2 state between 0 and 100 GeV. In the case of non-resonant production, the $a_{\text{non-res}}$= 0.2 effective coupling is excluded for a mass of the invisible spin-1 state between 0 and 650 GeV.

The monotop search in the hadronic channel will be considered in Run 2.

2.1.2. $tt + X$ final state

The main feature of this final state is two particles with the same electric charge. In order to exploit this point,it is essential to consider the events where both top quarks decay into leptons. The relevant final state probing this model is then $\ell^+\ell^+ + X$, where X depends on the exact process ($X = j + 2b$-jets for all diagrams of Figures 3 and 4 but the t-channel, $X = 2b$-jets for the t-channel of Figure 4). The cross-sections involving valence quarks are higher than the ones involving see quarks. Thus, the positively charged top quark pairs are largely more produced.

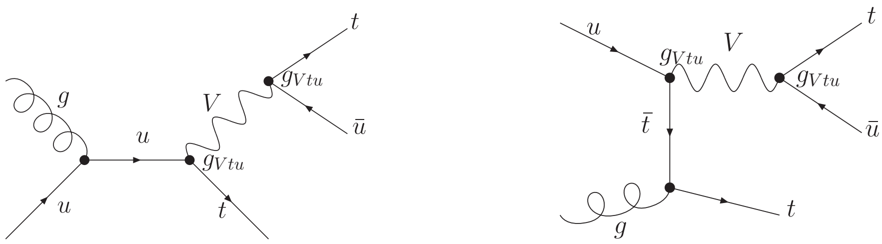

Figure 3: Feynman diagram of leading order processes leading to the $tt\bar{u}$ via the V production and its decay into $t\bar{u}$.

Figure 4: Feynman diagram of leading order processes leading to the $tt\bar{u}$ (left) and to the tt production (right), both via V exchange in the t-channel.

The typical background for this final state is mainly instrumental via a wrong charge reconstruction but can also be physical. Indeed, the $t\bar{t}V$ production can yield to a same-sign lepton pair together with b-jets. On the other hand, the $t\bar{t}$ production is large enough to make the charge mis-reconstruction rate relevant. Finally,"trident" electrons (photon radiation and conversion) can also contribute to this final state.

The Run 1 analysis exploiting the $\ell^+\ell^+ + b$–jets signature [5] is able to exclude a typical cross-section of 10 fb for a FCNC Higgs signal (similar to the tt production of Figure 4). Given the cross-sections of the described model, this final state is quite sensitive to a wide range of parameters.

There is one particular feature, not yet exploited, that can be used to extract the $tV(\to t\bar{u})$ production: the transverse momentum of the leading jet is quite high and will definitely help to disentangle the signal and the SM backgrounds, further increasing the sensitivity of this channel. As a consequence, the results shown in section 2.1.3 are quite conservative.

2.1.3. Combination of $tt + X$ and $t + E_{\mathrm{T}}^{\mathrm{miss}}$ analysis for the non-resonant production

The interesting point in combining the tt and $t + E_{\mathrm{T}}^{\mathrm{miss}}$ analysis is to cover invisible and the visible V decay simultaneously. The visible decay must be taken into account simply because V is produced from visible particles. More the production is large, more the visible decay should be relevant. In order to see the interplay, it is necessary to express the two constraints in the same parameter space.

Assuming that the phenomenology is fully described by σ_{tV}, σ_{tt}, $\sigma_{tt\bar{u}}^{\mathrm{virt}}$ and $\mathrm{BR}(V \to \chi\chi)$, the experimental cross-sections for each final state can be predicted:

$$\sigma_{t+E_{\mathrm{T}}^{\mathrm{miss}}} = \sigma_{tV} \times \mathrm{BR}(V \to \chi\chi) \qquad (5)$$

$$\sigma_{tt+X} = \sigma_{tV} \times \frac{1 - \mathrm{BR}(V \to \chi\chi)}{2} + \sigma_{tt\bar{u}}^{\mathrm{virt}} + \sigma_{tt} \qquad (6)$$

where σ_{tV} correspond to the 2 diagrams of Figure 3, $\sigma_{tt\bar{u}}^{\mathrm{virt}}$ (σ_{tt}) corresponds to the left (right) diagram of Figure 4.IMPORTANT COMMENT: this split is in principle not correct, but needed. Not correct because all $gu \to tt\bar{u}$ amplitudes must interfere. Needed because only the real production is scaled by $\mathrm{BR}(V \to \chi\chi)$, in which we are precisely interested. This needs to be further discussed with theorists. The factor 2 comes from the fact that $\mathrm{BR}(V \to t\bar{u}) = \mathrm{BR}(V \to \bar{t}u)$. In practice, the selection efficiency will be different for each process, since they have quite different topology. We neglect this aspect in this simplified discussion.

If we neglect the term $\sigma_{tt\bar{u}}^{\mathrm{virt}} + \sigma_{tt}$ in equation (6), it becomes easy to compute the excluded area in the plane $(\sigma_{tV}, \mathrm{BR}(V \to \chi\chi))$ by each of the channel. Considering the excluded cross-section in the monotop analysis ($\sigma_{t+E_{\mathrm{T}}^{\mathrm{miss}}}^{\mathrm{excl}}$) and in the same-sign top analysis ($\sigma_{tt+X}^{\mathrm{excl}}$), it comes:

$$\left(\sigma_{tV}^{\mathrm{excl}}\right)_{\mathrm{monotop}} > \frac{\sigma_{t+E_{\mathrm{T}}^{\mathrm{miss}}}^{\mathrm{excl}}}{\mathrm{BR}(V \to \chi\chi)} \qquad (7)$$

$$\left(\sigma_{tV}^{\mathrm{excl}}\right)_{\mathrm{sstop}} > \frac{2 \times \sigma_{tt+X}^{\mathrm{excl}}}{1 - \mathrm{BR}(V \to \chi\chi)} \qquad (8)$$

According to the monotop and same-sign top analysis performed during the Run 1, the cross-sections limits for $m_V \sim 500$ GeV are:

$$\sigma^{\text{excl}}_{t+E_T^{\text{miss}}} \times \text{BR}(W \to \ell\nu_\ell) \sim 250 \text{ fb} \quad (9)$$

$$\sigma^{\text{excl}}_{tt+X} \sim 10 \text{ fb} \quad (10)$$

By putting these numbers into equations (7) and (8) ($\text{BR}(W \to \ell\nu_\ell)$ include electrons and muons only and is taken at 21.3%), we obtain the excluded areas in the $(\sigma_{tV}, \text{BR}(V \to \chi\chi))$ plane for each analysis as shown in figure 5. The power of the same-sign signature offers a nice way to complete the monotop analysis for $\text{BR}(V \to \chi\chi) \lesssim 0.98$ and to exclude a much larger part of the parameter space.

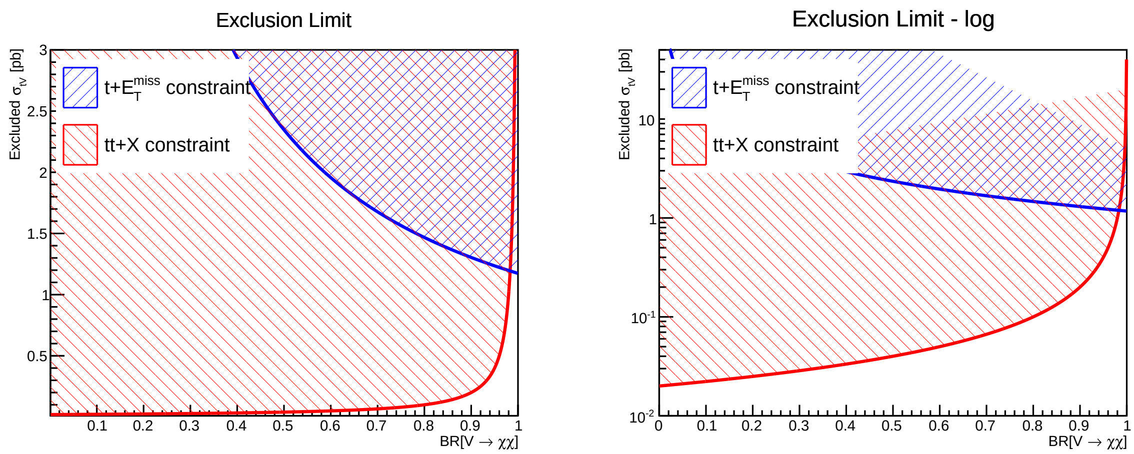

Figure 5: All cross-sections above the curves are excluded cross-section by the monotop analysis (blue) and the $\ell^+\ell^+$ (red) as a function of $\text{BR}(V \to \chi\chi)$. For $\text{BR}(V \to \chi\chi) \lesssim 0.98$, the monotop only excludes large cross-sections while the $\ell^+\ell^+$ takes over in order to recover some sensitivity.

In practice, equations (5) and (6) show that figure 5 underestimate the sensibility of the $tt + X$ analysis since the terms $\sigma^{\text{virt}}_{tt\bar{u}}$ and σ_{tt} were neglected. The additional sensitivity brought by these terms might depend on the event selection, due to the different event topology (for instance, leading jet softer). Also, the way to interpret the two analysis in the same parameter plane becomes less obvious when $\sigma^{\text{virt}}_{tt\bar{u}}$ and σ_{tt} are involved. In this case, the couplings g^R_{Vtu} and m_V might be a good option but this has to be properly defined Need discussion with theorists.

2.2. Relevant model parameters

Which parameters impact the kinematics (this is the only relevant aspect form the experimental point of view)? Some studies would be nice to put in this documents about:

- mediator mass
- mediator width → no effect (or parametrizable effects, plots are ready and need to be included)
- **which parameters** impact our experimental sensitivity? Which plane should be scanned?

What are the relevant numerical range to explore? First guess would be to follow the mono-top analysis.

2.3. Practical implementation

ATLAS has considered two models, a resonant and a non-resonant production, using only right-handed top quarks in the lepton+jets final state. The signal samples were produced with MADGRAPH5 v1.5.11 interfaced with PYTHIA 8.175, using the MSTW2008LO Parton Distribution Function (PDF) set (lhapdf ID: 21000). The mass of the top quark was set at 172.5 GeV. Dynamic renormalisation and factorisation scales were used. The E_T^{miss} particle mass was varied, and in the case of the resonant model the resonance mass was fixed at 500 GeV:

- Resonant model, E_T^{miss} particle mass: [0,100] GeV in 20 GeV steps
- Non-resonant model, E_T^{miss} particle mass: [0,150] GeV in 25 GeV steps, [200,300] GeV in 50 GeV and [400,1000] GeV in 100 GeV steps

The couplings a_{res} and $a_{non\text{-}res}$ are set at a fixed value of 0.2. In addition, two samples are produced for the resonant model for $m(f_{met}) = 100$ GeV, with coupling strengths fixed at $a_{res} = 0.5$ and $a_{res} = 1.0$, in order to check the effect of the resonance width on the signal event kinematics. The total width of the resonance varies quadratically with the coupling strength, corresponding to a width of 3.5 GeV, 21.6 GeV, and 86.5 GeV at $a_{res} = 0.2$, $a_{res} = 0.5$, and $a_{res} = 1.0$, respectively.

The number of free parameters is reduced by assuming $(a^q_{res})_{12} = (a^q_{res})_{21} = (a^{1/2}_{res})_3 \equiv a_{res}$ for the resonant model and $(a_{non\text{-}res})_{13} = (a_{non\text{-}res})_{31} \equiv a_{non\text{-}res}$ for the non-resonant model, all other elements of these coupling matrices being equal to 0. For each model, the coupling parameter a_{res} or $a_{non\text{-}res}$ and the masses of the exotic particles are independent.

The cross-sections as well as the width of the resonance for the resonance model are shown in Table 1. The cross-section is slowly decreasing when $m(f_{met})$ increases, and the values do not differ by larger than 10%, due to the similarity of the kinematics, in the chosen mass range.

$m(f_{met})$ [GeV]	σ_{lep} [pb]	σ_{had} [pb]	$\Gamma(\Phi)$ [GeV]
0	1.107	2.214	3.492
20	1.102	2.205	3.491
40	1.089	2.180	3.487
60	1.068	2.137	3.481
80	1.039	2.078	3.472
100	1.001	2.003	3.461
100 ($a_{res} = 0.5$)	6.091	12.13	21.63
100 ($a_{res} = 1.0$	21.77	43.72	86.52

Table 1: Theoretical predictions for the product of the production cross-section of the scalar resonance, the branching ratio of its decay into a top quark and the invisible particle, and of the branching ratio of the top quark decay into a semi-leptonic (σ_{lep}) or fully-hadronic (σ_{had}) final state, in the resonance model. Values are given for a resonance of mass 500 GeV and for an effective coupling $a_{res} = 0.2$ (except for two masses), as a function of the mass $m(f_{met})$ of the neutral fermion. The total widths $\Gamma(\Phi)$ of the resonance are also shown.

For the non-resonant case, the cross-sections are given in Table 2 and are calculated with $a_{non\text{-}res} = 0.2$. The cross-section diverges when $m(v_{met})$ tends to 0 GeV. However, when the mass is exactly 0 GeV the cross-section has a finite value, due to the specificity of the propagator for this massless spin-1 boson.

$m(v_{met})$ [GeV]	σ_{lep} [pb]	σ_{had} [pb]
0	96.03	192.4
25	359.0	717.9
50	113.4	226.9
75	59.86	119.5
100	37.45	74.82
125	25.35	50.68
150	18.00	35.96
200	9.662	19.28
250	5.506	11.02
300	3.328	6.656
400	1.372	2.738
500	0.6345	1.270
600	0.3192	0.6354
700	0.1698	0.3383
800	0.09417	0.1883
900	0.05472	0.1091
1000	0.03259	0.06479

Table 2: Theoretical predictions for the product of the production cross-section of the invisible vector v_{met} and of a top quark, and of the branching ratio of the top quark decay into a semi-leptonic (σ_{lep}) or fully-hadronic (σ_{had}) final state, in the non-resonance model. Values are given for an effective coupling $a_{\text{non-res}} = 0.2$, as a function of the mass $m(v_{met})$ of the invisible state.

I think it might make more sense to have the joboption information in a public web site instead of adding all the details into the note. Reference only visible for ATLAS members: https://svnweb.cern.ch/trac/atlasoff/browser/Generators/MC12JobOptions/trunk/gencontrol/MadGraphControl_Monotop.py

Question for DM forum:

- Do we want to give more details about the Madgraph implementation, the couplings value in the param_card, etc ... ?
- I am not aware of any work on systematic variation due to scale, PDF choice, showering (Maybe some was done in the monotop analysis?). Then I am not completely what to put here.

References

[1] J. Andrea, B. Fuks and F. Maltoni, *Monotops at the LHC*, Phys.Rev. **D84** (2011) 074025, arXiv: 1106.6199 [hep-ph].

[2] I. Boucheneb et al., *Revisiting monotop production at the LHC* (2014), arXiv: 1407.7529 [hep-ph].

[3] B. Fuks, *Monotop Effective Theory: MadGraph model*, http://feynrules.irmp.ucl.ac.be/wiki/Monotops.

[4] *Search for a single-top quark produced in association with missing energy in proton-proton collisions at* $\sqrt{s} = 8$ TeV *with the ATLAS detector*, Eur. Phys. J. C **75:79** (2015), arXiv: 1410.5404 [hep-ex].

[5] *Analysis of events with b-jets and two leptons of the same charge or three leptons in pp collisions at* $\sqrt{s} = 8$ *TeV with the ATLAS detector*, To be submitted to Eur. Phys. J. C (2015).

Appendix

A. Cross-sections

Figure 6 shows the different cross-section contributing to the same-sign top quark pair production, as a function of the mediator mass. The elementary processes involved in the cross-section calculation are shown in figure 7.

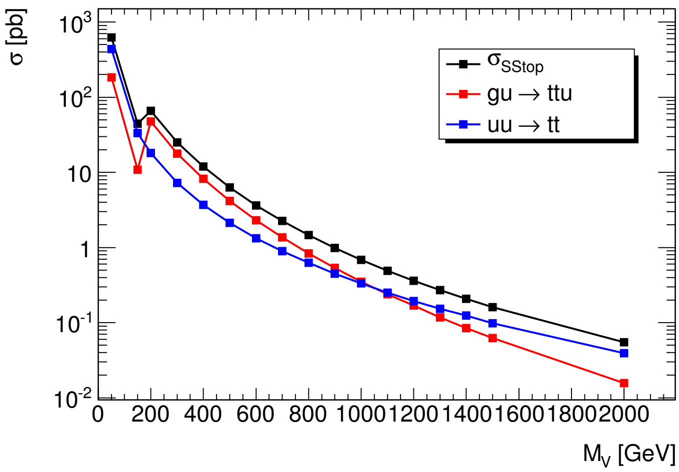

Figure 6: Total cross-section of $tt\bar{u}$ (red) and tt (bleue) production for different mediator mass. The total cross-section is shown in black.

Figure 8 shows how the various diagrams contribute to the total cross-section for the $tt + X$ final state, as a function of the mediator mass and for two different width. More precisely, there are two disctinct partonic processes: $gu \to tt\bar{u}$ ($\sigma(tt\bar{u})$) and $uu \to tt$ ($\sigma(tt)$). The total cross-section is written $\sigma(tt+X) \equiv \sigma(tt\bar{u}) + \sigma(tt)$. The width which are considered in this section are the value calculated by MadGraph (labelled *auto*) using the visible decay mode only, and a value set by hand at 10% of m_V.

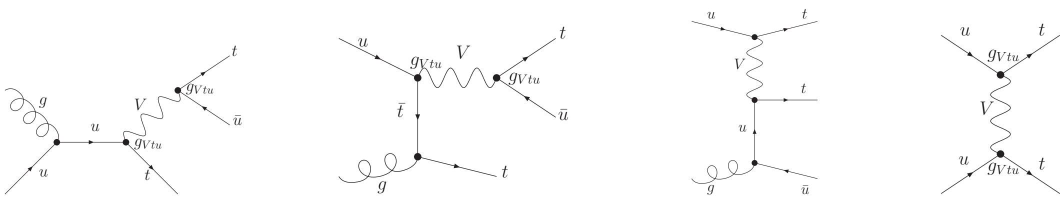

Figure 7: Feynman diagram of leading order processes leading to the $tt\bar{u}$ (left) and to the tt production (right), both via V exchange in the t-channel.

The left plot of figure 8 shows the fraction $\sigma(tt)/\sigma(tt+X)$ as a function of m_V. The observed behaviour is explained by the propagator of V: below the m_t threshold, V can only be virtual and the t-channel has a large contribution. At high mass, it becomes more and more difficult to produce an on-shell V which makes the t-channel fraction larger as the mass increases. This is even more pronounced when Γ_V increases since it makes the probability to be virtual higher.

The right plot of figure 8 shows the impact of third diagram from figure 7 on the $tt\bar{u}$ production. Indeed, V doesn't decay into $t\bar{u}$ in this diagram, in opposition to the diagrams describing $gu \to tV(\to t\bar{u})$. Practically, the fraction of $gu \to tt\bar{u}$ events with an on-shell V[3] compared to all $gu \to tt\bar{u}$ events. More the V width is large, more this effect is visible. The interest of this plot is to quantify the fraction of events which cannot be simply scaled by BR$(V \to \chi\chi)$ for the monotop and same-sign combination (cf. 2.1.3).

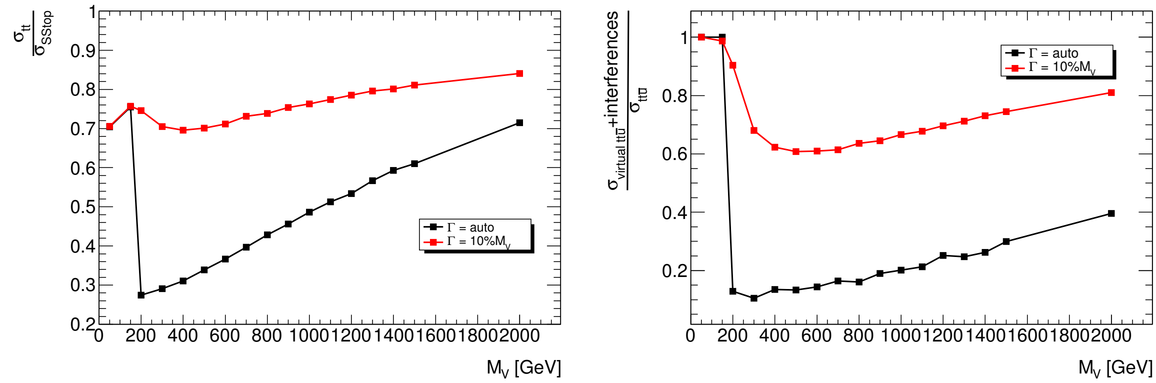

Figure 8: Fraction of t-channel for the $tt + X$ final state as a function of the mediator mass (left) and effect of virtual V contribution to $gu \to tt\bar{u}$ process as a function of the mediator mass (right).

[3] This is defined by a Madgraph parameter $bwcut$, standing for Breit-Wigner Window. If $\sqrt{E_V^2 - \vec{p}_V^2}$ is in a window of $bwcut \times \Gamma_V$ centered to m_V, then V is considered as on-shell. For this study, $bwcut = 25$.

B. Mediator width effects for the non-resonant model

B.1. Effects on the tV production

Figure 10 and 11 shows the V mass distribution, the transverse momentum for V and for the top quark coming from $V \to t\bar{u}$, for different masses and V width. These figures are relevant independtly of the V decay mode (visible or invisible). It applies then for both monotop and same-sign top final states.

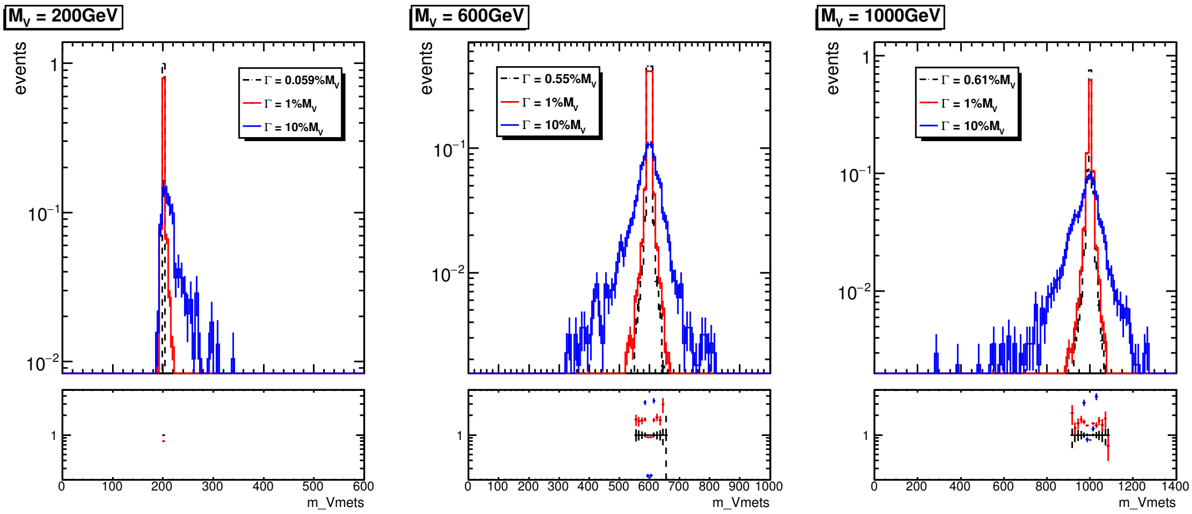

Figure 9: Distribution of V invariant mass for the $gu \to tV(\to t\bar{u})$ (on-shell V) for $m_V = \{200, 600, 1000\}$ GeV (from left to right) and for three different visible decay width (computed from Madgraph directly, 1% and 10%).

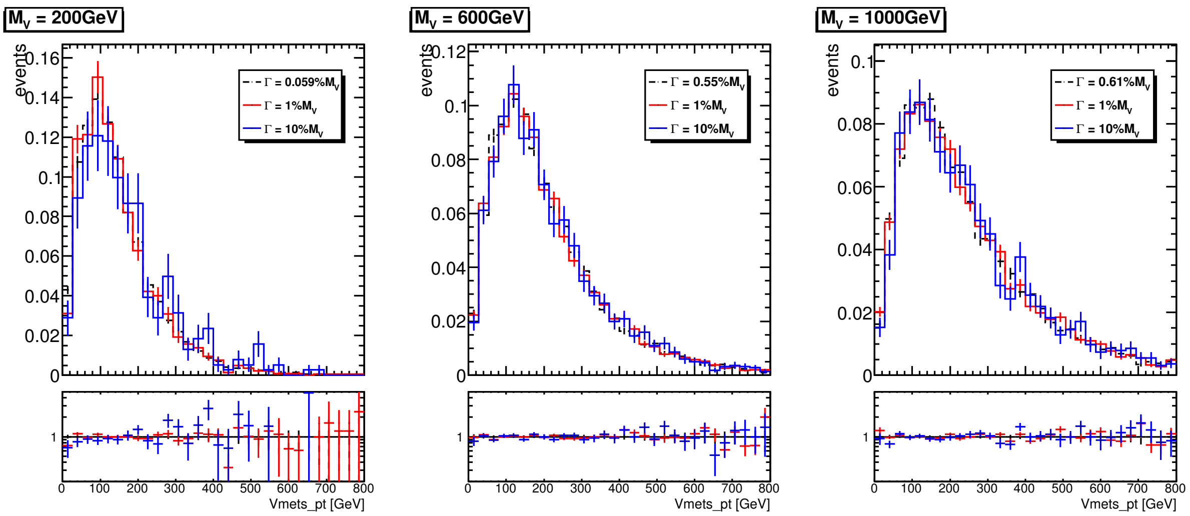

Figure 10: Distribution of the V p_T for the $gu \to tV(\to t\bar{u})$ (on-shell V) for $m_V = \{200, 600, 1000\}$ GeV (from left to right) and for three different visible decay width (computed from Madgraph directly, 1% and 10%).

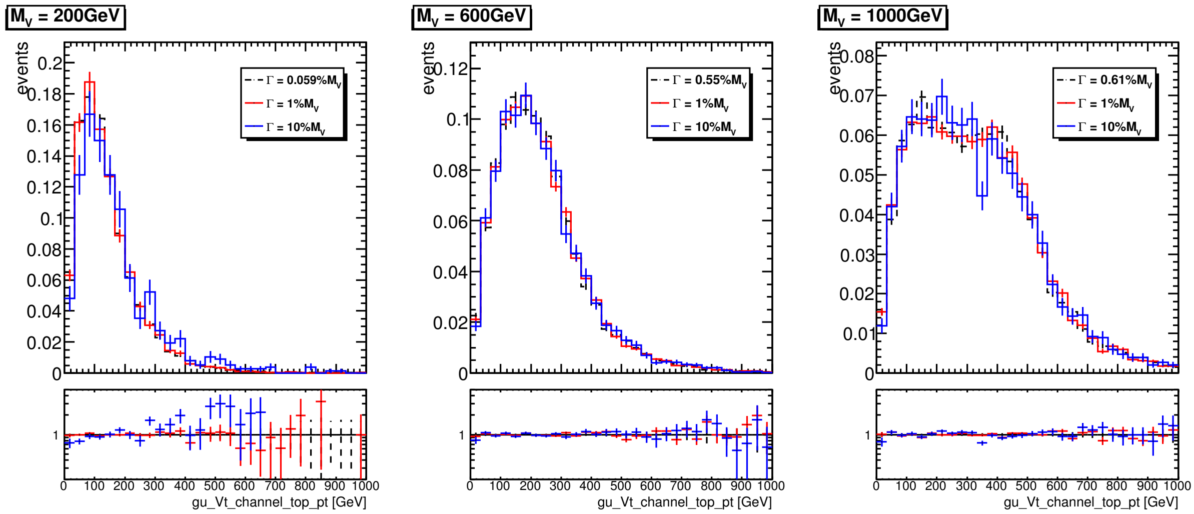

Figure 11: Distribution of the top quark p_T coming from the V decay for the $gu \rightarrow tV(\rightarrow t\bar{u})$ (on-shell V) for $m_V = \{200, 600, 1000\}$ GeV (from left to right) and for three different visible decay width (computed from Madgraph directly, 1% and 10%).

B.2. Effects on the $tt + X$ final state

Figures 12 to 25 focus on the $tt + X$ production showing the p_T of all top quarks in the events, the leading jet p_T, the jet multiplicity, the $E_{\mathrm{T}}^{\mathrm{miss}}$, the lepton multiplicity and H_T. These plots show that with V width has a clear impact on some important distributions (top quark p_T, leading jet p_T, jet multiplicity, H_T). Section B.3 will demonstrate this impact is just a consequence of how the width change the relative fraction of each diagrams of Figure 7.

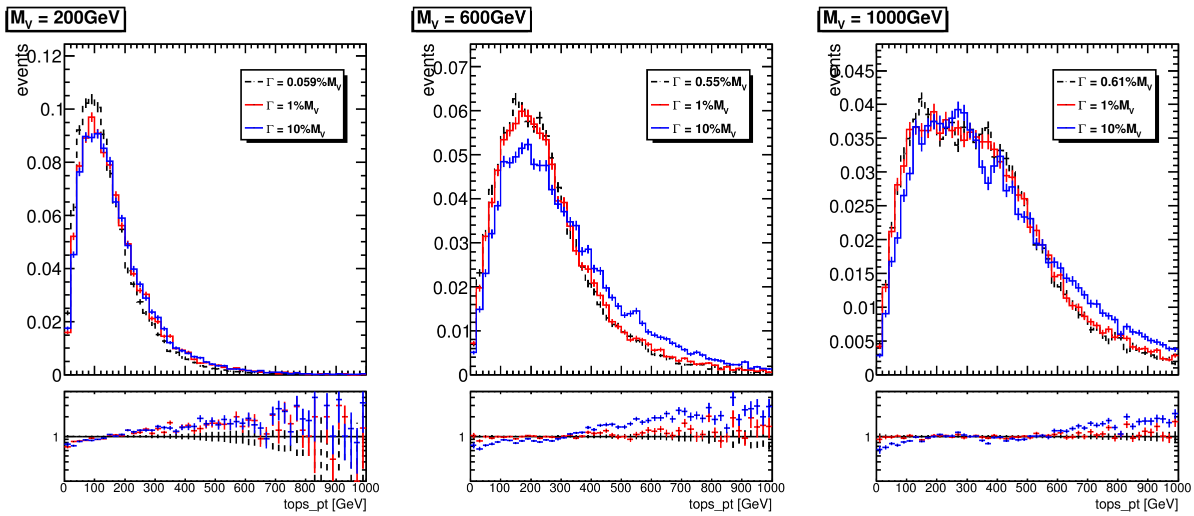

Figure 12: Distribution of all top quark p_T in the events for all processes leading to $tt + X$ for $m_V = \{200, 600, 1000\}$ GeV (from left to right) and for three different visible decay width (computed from Madgraph directly, 1% and 10%).

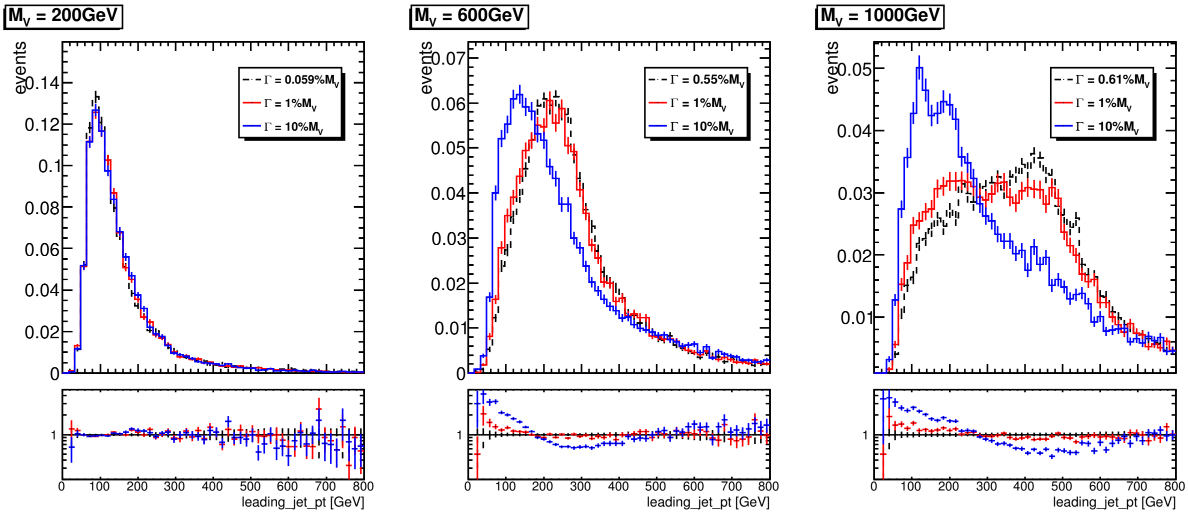

Figure 13: Distribution of the leading jet p_T for all processes leading to $tt + X$ for $m_V = \{200, 600, 1000\}$ GeV (from left to right) and for three different visible decay width (computed from Madgraph directly, 1% and 10%).

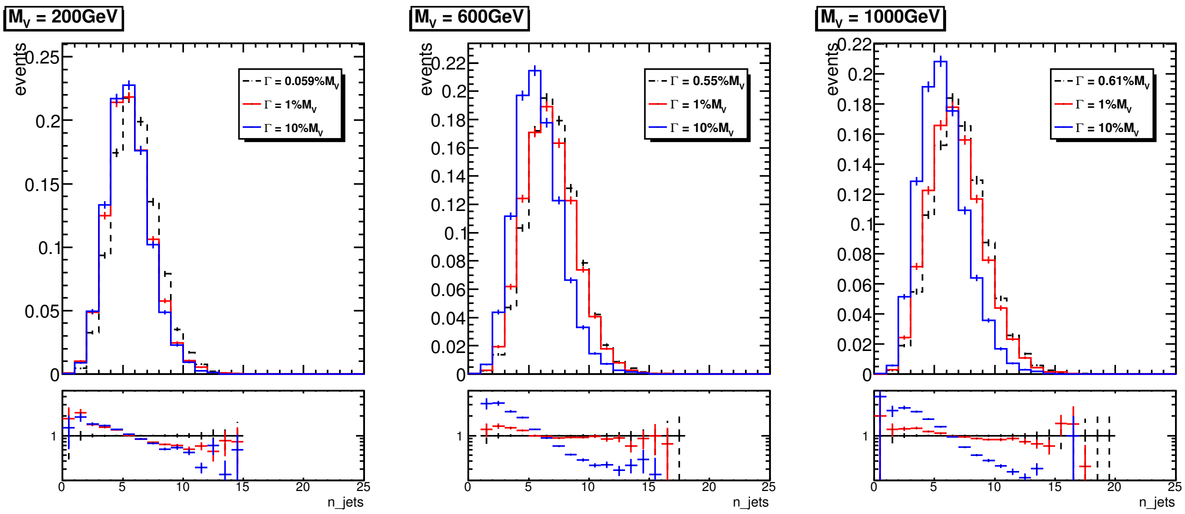

Figure 14: Distribution of the jet multiplicity for all processes leading to $tt + X$ for $m_V = \{200, 600, 1000\}$ GeV (from left to right) and for three different visible decay width (computed from Madgraph directly, 1% and 10%).

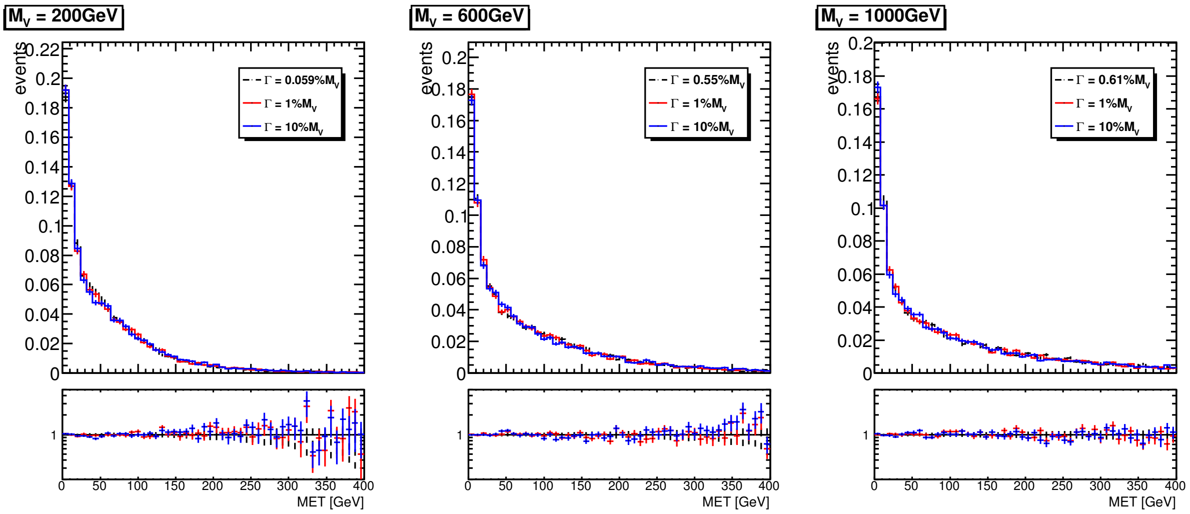

Figure 15: Distribution of the $E_{\mathrm{T}}^{\mathrm{miss}}$ for all processes leading to $tt + X$ for $m_V = \{200, 600, 1000\}$ GeV (from left to right) and for three different visible decay width (computed from Madgraph directly, 1% and 10%).

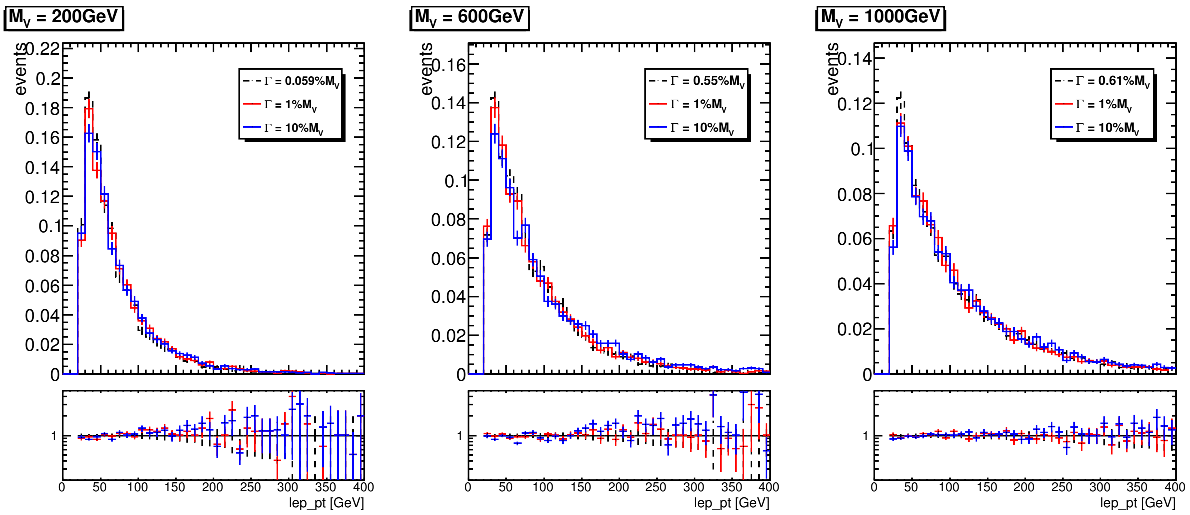

Figure 16: Distribution of the lepton p_T for all processes leading to $tt + X$ for $m_V = \{200, 600, 1000\}$ GeV (from left to right) and for three different visible decay width (computed from Madgraph directly, 1% and 10%).

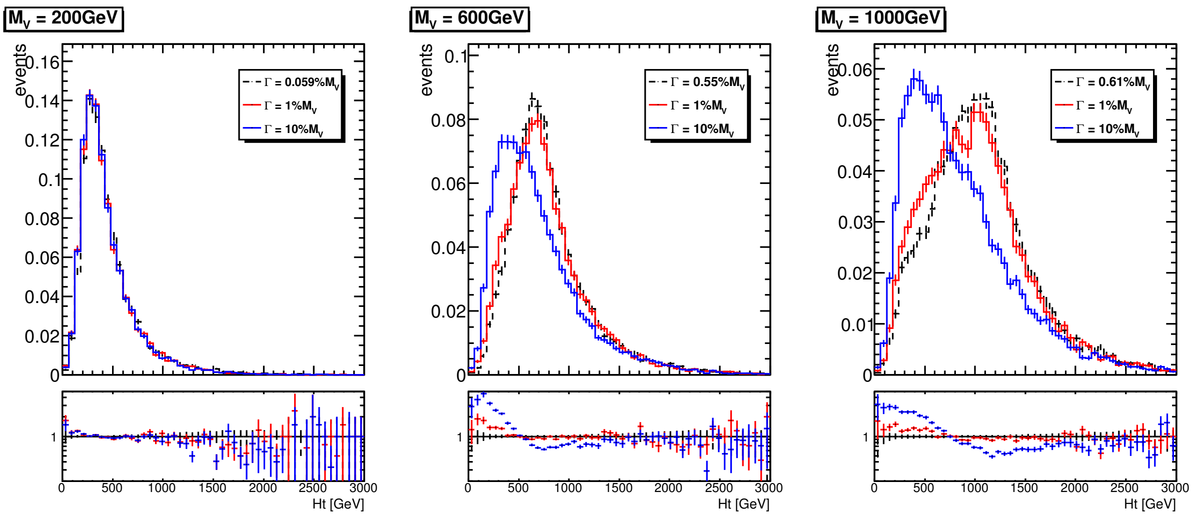

Figure 17: Distribution of the p_T scalar sum (H_T) for all processes leading to $tt + X$ for $m_V = \{200, 600, 1000\}$ GeV (from left to right) and for three different visible decay width (computed from Madgraph directly, 1% and 10%).

B.3. Comparison of $gu \to tV(\to t\bar{u})$ and $uu \to tt$ processes

Figures 18 to 21 show the width effect on top p_T, leading jet p_T, jet multiplicity and H_T, separately for $gu \to tV(\to t\bar{u})$ and $uu \to tt$ processes. These plot show the important kinematic differences between the tt production via a t-channel exchange of the mediator and the direct production of the mediator, decaying into $t\bar{u}$. On each of these process, the width doesn't change at all the kinematics but it does change the relative importance of each process, as shown in section A. This explains then the width impact observed in section B.2.

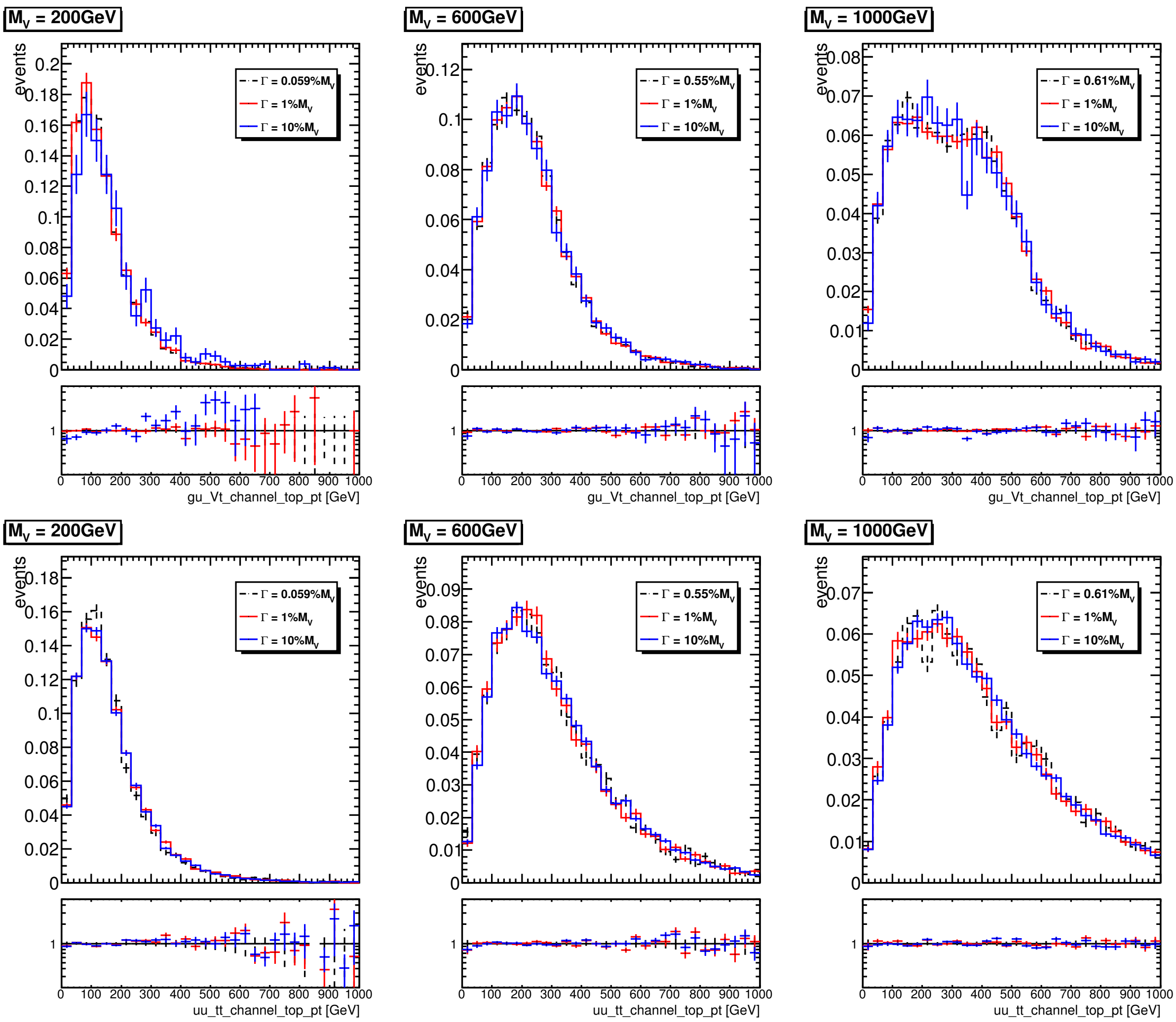

Figure 18: Distribution of all top quark p_T in the events for all processes leading to $tt + X$ for $m_V = \{200, 600, 1000\}$ GeV (from left to right) and for three different visible decay width (computed from Madgraph directly, 1% and 10%). Top plots show $gu \to tt\bar{u}$ and bottom plots show $uu \to tt$.

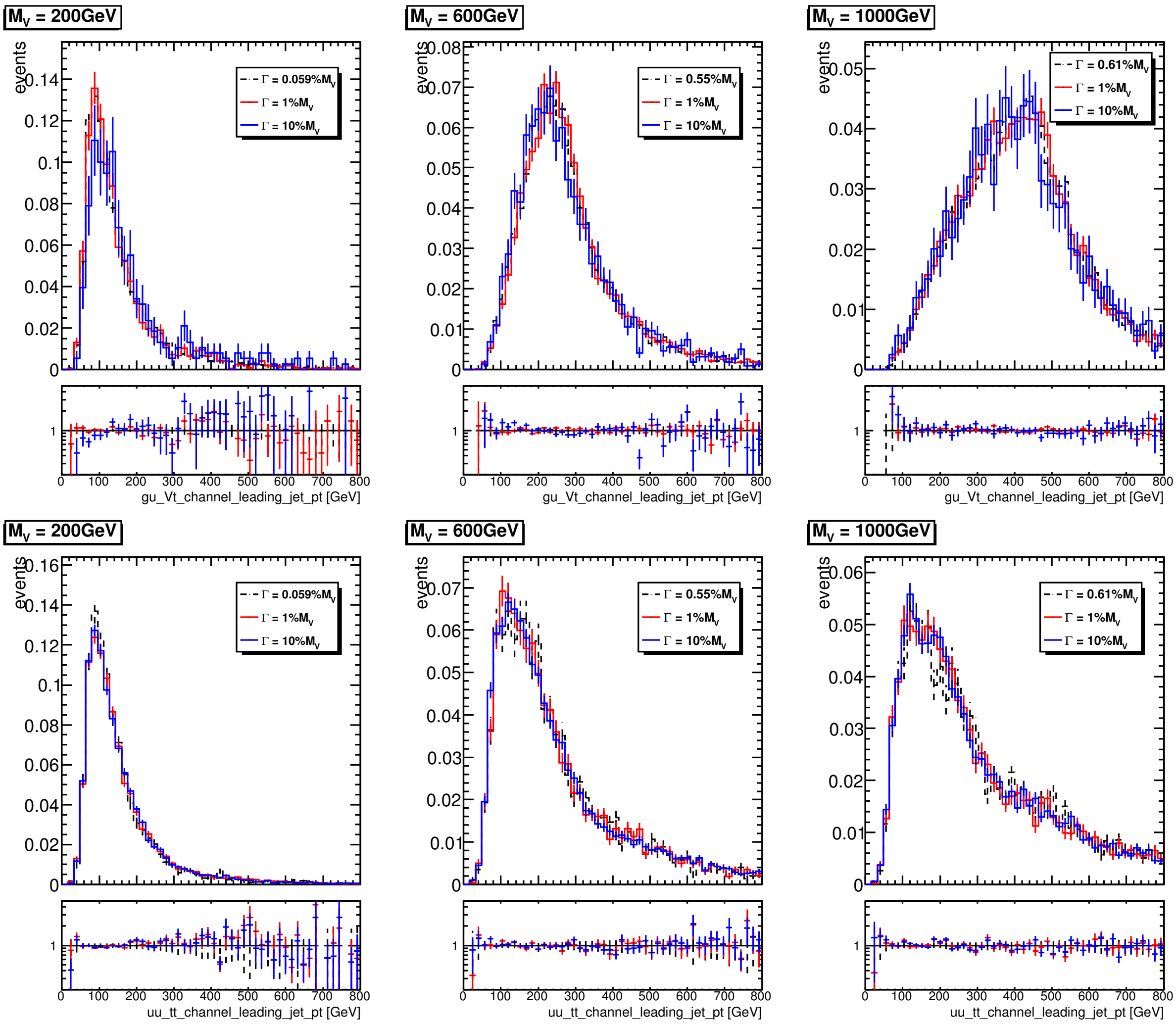

Figure 19: Distribution of the leading jet p_T for all processes leading to $tt + X$ for $m_V = \{200, 600, 1000\}$ GeV (from left to right) and for three different visible decay width (computed from Madgraph directly, 1% and 10%). Top plots show $gu \to tt\bar{u}$ and bottom plots show $uu \to tt$.

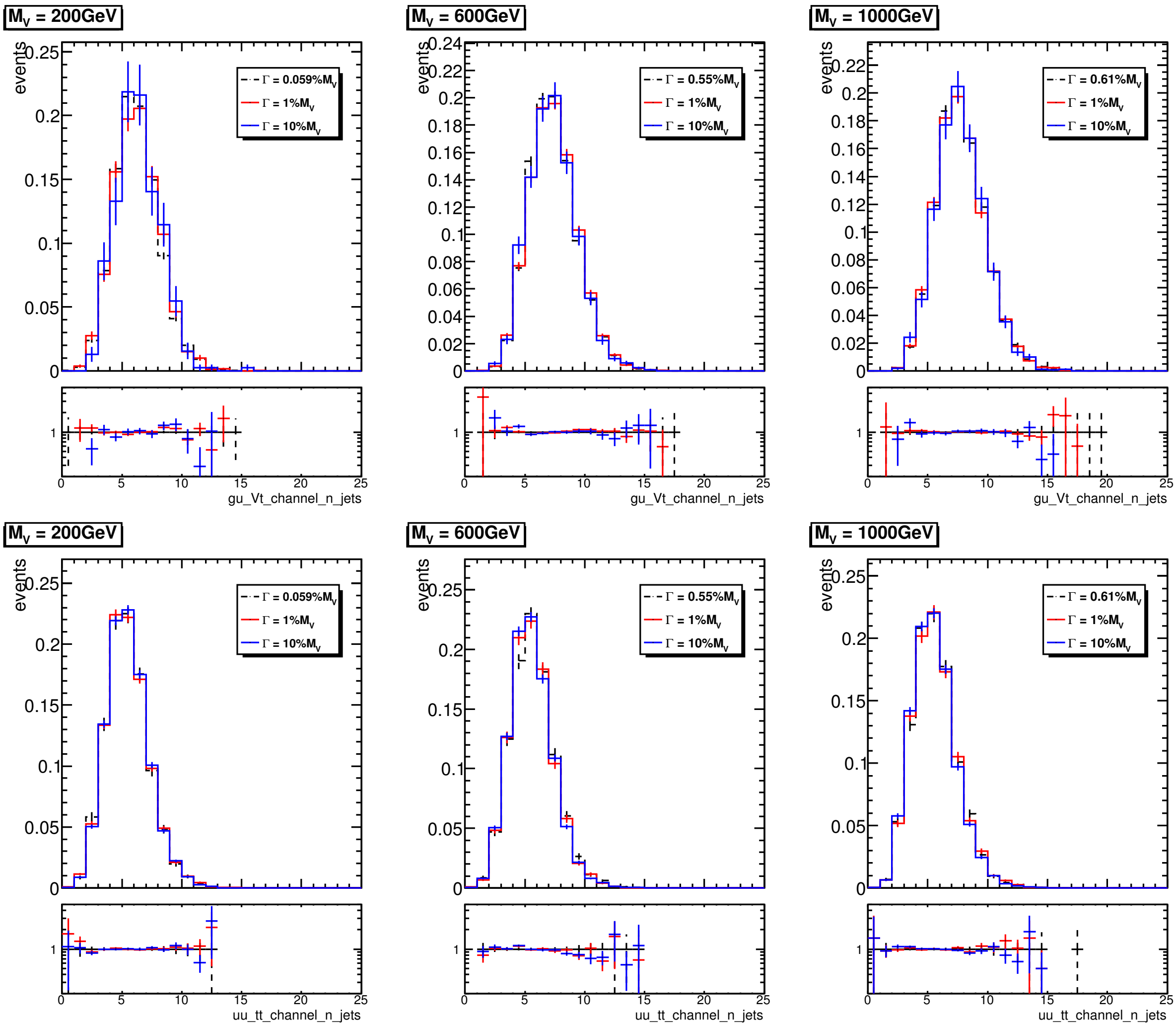

Figure 20: Distribution of the jet multiplicity for all processes leading to $tt + X$ for $m_V = \{200, 600, 1000\}$ GeV (from left to right) and for three different visible decay width (computed from Madgraph directly, 1% and 10%). Top plots show $gu \to tt\bar{u}$ and bottom plots show $uu \to tt$.

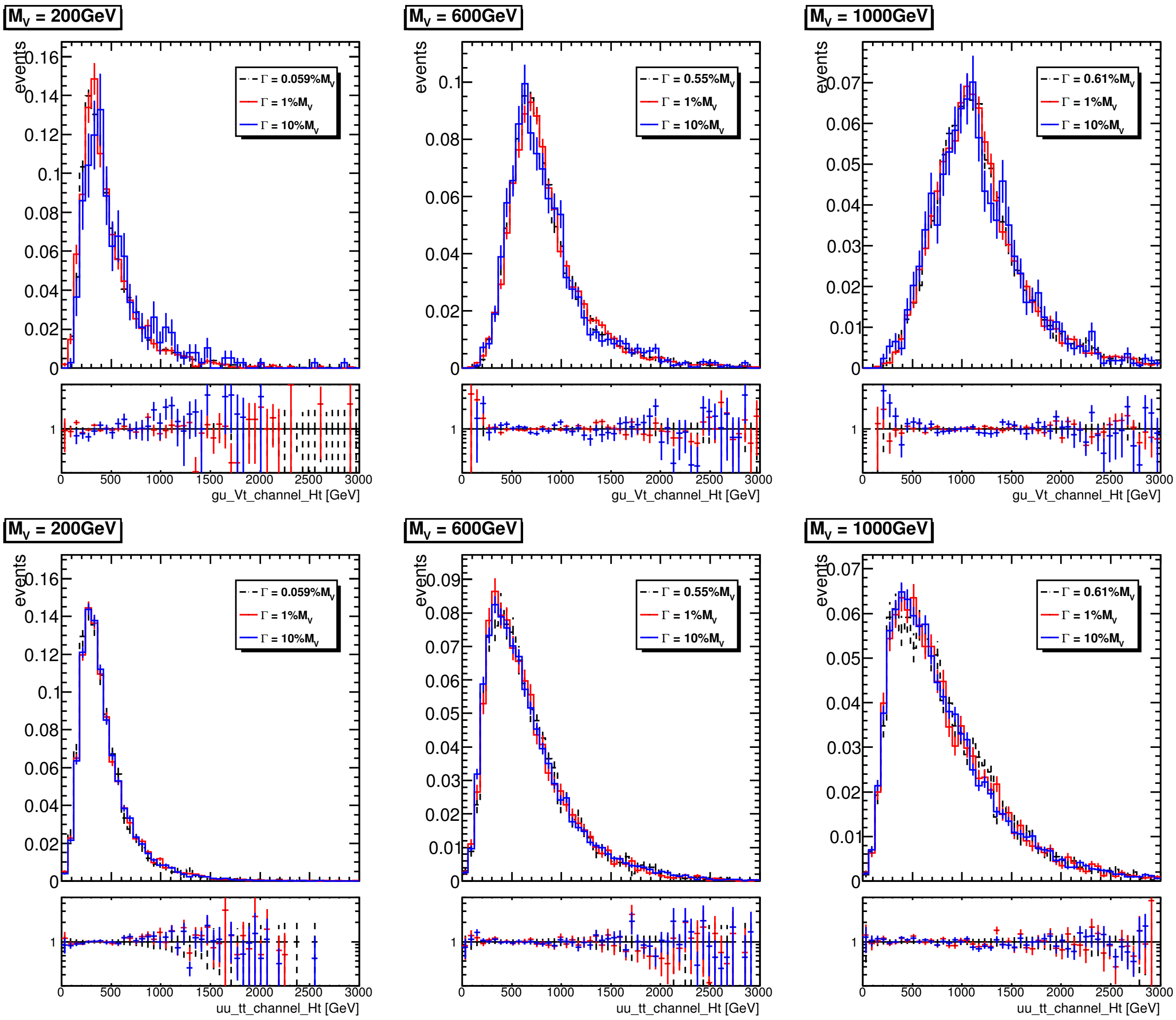

Figure 21: Distribution of the p_T scalar sum (H_T) for all processes leading to $tt+X$ for $m_V = \{200, 600, 1000\}$ GeV (from left to right) and for three different visible decay width (computed from Madgraph directly, 1% and 10%). Top plots show $gu \rightarrow tt\bar{u}$ and bottom plots show $uu \rightarrow tt$.

C. Signal and background distributions ($tt + X$ final state)

In this section, the shape of some key distributions are compared for for the two signal processes, namely $gu \to tt\bar{u}$ and $uu \to tt$, and the two main backgrounds relevant for the $tt + X$ final state, namely $t\bar{t}$ (via charge mis-reconstruction) and $t\bar{t} + V$. The distributions are obtained at the truth hadronic level, without any detector effects. The objects are selected using criteria close from those used in the Run 1 analysis.

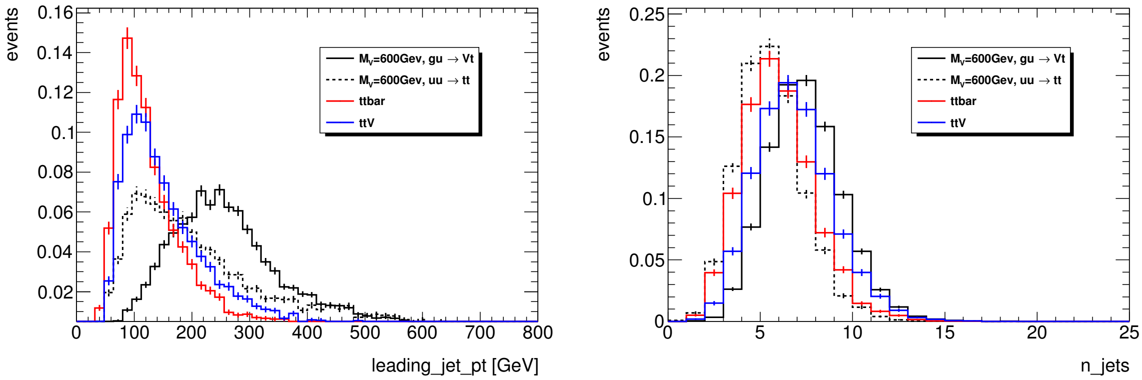

Figure 22: Distribution of the leading jet p_T for signals ($m_V = 600$ GeV, Γ_V computed in MadGraph) and backgrounds at the (hadronic) thruth level.

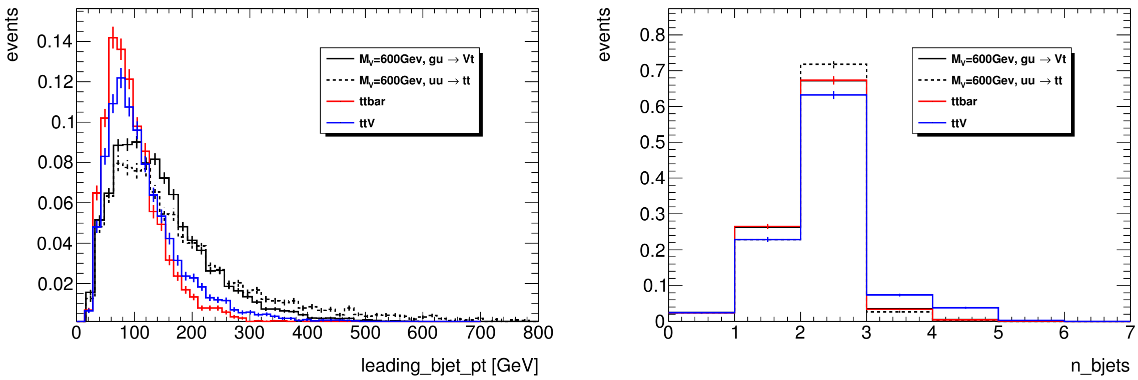

Figure 23: Distribution of the leading jet p_T for signals ($m_V = 600$ GeV, Γ_V computed in MadGraph) and backgrounds at the (hadronic) thruth level.

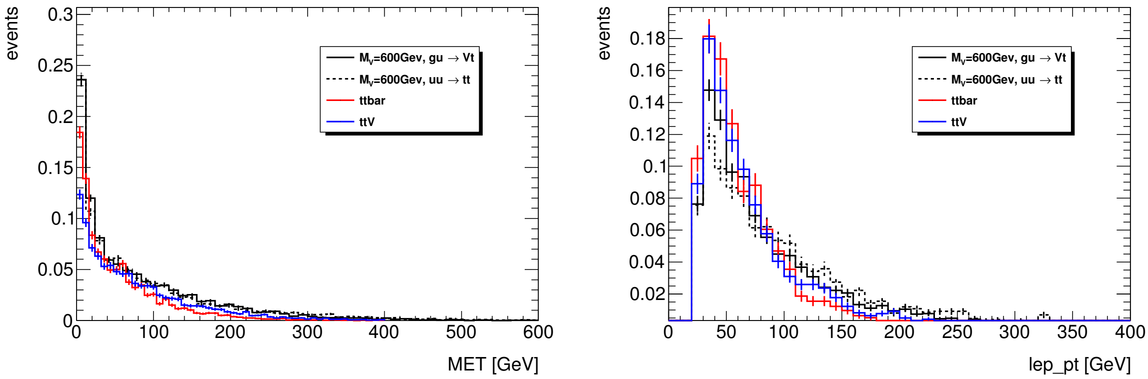

Figure 24: Distribution of the $E_{\mathrm{T}}^{\mathrm{miss}}$ for signals ($m_V = 600$ GeV, Γ_V computed in MadGraph) and backgrounds at the (hadronic) thruth level.

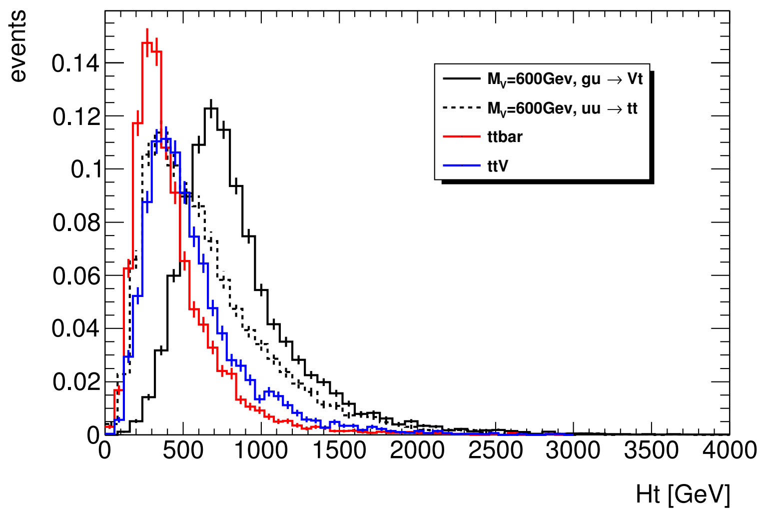

Figure 25: Distribution of the p_T scalar sum (H_T) for signals ($m_V = 600$ GeV, Γ_V computed in MadGraph) and backgrounds at the (hadronic) thruth level.